

# Soot and charcoal as reservoirs of extracellular DNA

S. Jelavić,<sup>a,b\*</sup> L.G. Thygesen,<sup>c</sup> V. Magnin,<sup>b</sup> N. Findling,<sup>b</sup> S. Müller,<sup>d</sup> V. Meklesh,<sup>e</sup> K.K. Sand<sup>a</sup>

<sup>a</sup>Centre for Geogenetics, GLOBE Institute, University of Copenhagen, Øster Voldgade 5–7, 1350 Copenhagen, Denmark.

<sup>b</sup>Université Grenoble Alpes, Université Savoie Mont Blanc, CNRS, IRD, Université Gustave Eiffel, ISTerre, F-38000 Grenoble, France.

<sup>c</sup>University of Copenhagen, Department of Geoscience and Natural Resource Management, Rolighedsvej 23, 1958 Frederiksberg C, Denmark.

<sup>d</sup>University of Copenhagen, Department of Geosciences and Natural Resource Management, Øster Voldgade 10, 1350 Copenhagen K, Copenhagen, Denmark.

<sup>e</sup>Centre for Environmental and Climate Science, Lund University, Sölvegatan 37, 223 62 Lund, Sweden.

\*corresponding author: stanislav.jelavic@univ-grenoble-alpes.fr

## ABSTRACT

The vast potential of using sediment adsorbed DNA as a window to past and present biodiversity rely on the ability of solid surfaces to adsorb environmental DNA. However, a comprehensive insight into DNA adsorption at surfaces in general is lacking. Soot and charcoal are carbonaceous materials widespread in the environment where they readily can come in contact with extracellular DNA shed from organisms. Using batch adsorption, we measured DNA adsorption capacity at soot and charcoal as a function of solution composition, time and DNA length. We observed that the adsorption capacity for DNA is highest at low pH, that it increases with solution concentration and cation valency and that the activation energy for DNA adsorption at both soot and charcoal is  $\sim 50 \text{ kJmol}^{-1}$ , suggesting strong binding. We demonstrate how the interaction between DNA and soot and charcoal partly occurs via terminal base pairs, suggesting that, besides electrostatic forces, hydrophobic interactions play an important role in binding. The large adsorption capacities and strong binding of DNA to soot and charcoal are features important for eDNA research and provide a motivation for use of carbonaceous materials from, e.g. anthropogenic pollution or wildfire as sources of biodiversity information.

## INTRODUCTION

Environmental DNA (eDNA) is genetic information shed from living or deceased organisms into their surroundings. Free extracellular eDNA degrades in matter of days but when adsorbed to minerals in sediments, it can be preserved for thousands of years.<sup>1,2</sup> The adsorptive protection provided by minerals is likely a result of disrupted molecular recognition of adsorbed DNA by enzymes<sup>3,4</sup> and the inactivation of enzymes by adsorption to the same surfaces.<sup>5</sup> Once adsorbed, the eDNA can be transported across time and space following sedimentary processes. Consequently, mineral stored eDNA is a unique resource of information relevant for estimating past and present biodiversity,<sup>6</sup> monitoring of invasive and endangered species<sup>7</sup> and for reconstruction of paleoenvironments.<sup>8</sup> Given that eDNA can be extracted from water, sediments<sup>9</sup> and air,<sup>10,11</sup> the contribution of common non-

41 mineral environmental surfaces such as carbonaceous materials (CM) to the environmental reservoir  
42 of DNA is unclear.

43 CMs are produced anthropogenically and naturally by burning fossil fuels and vegetation. CMs are  
44 ubiquitous in soils and, because of their low density and small size, they are easily transported by air  
45 to aqueous environments including freshwater and marine sediments.<sup>12</sup> The abundance, easy  
46 transportation and widespread occurrence renders soot and charcoal as promising reservoirs of eDNA.  
47 Incomplete combustion of fossil fuels produces soot while burning of vegetation produces both  
48 charcoal by pyrolysis and soot by combustion and condensation of gases within fire. There is a great  
49 variability in structure and composition of soot and charcoal depending on their source materials and  
50 temperature of formation.<sup>12,13</sup> In general, both can be envisaged as polycyclic aromatic materials built  
51 from agglomerates of ordered graphitic domains consisting of sp<sup>2</sup>-hybridised carbon and domains that  
52 deviate from a perfect graphitic structure with an increased incorporation of oxygen and hydrogen.<sup>14–</sup>  
53 <sup>16</sup> An important difference is that the graphitic domains in soot can occur at relatively lower  
54 temperatures<sup>13</sup> than charcoal<sup>17</sup> and that charcoal can contain a core of unburnt biomass.

55 Knowledge of the binding between the DNA and CMs is important for understanding the adsorption  
56 under various environmental conditions. Extracellular eDNA is principally double stranded DNA  
57 (dsDNA) since this form is more resistant to degradation than single stranded DNA.<sup>18–21</sup> Studies of the  
58 interaction between dsDNA and materials compositionally and structurally similar to soot and  
59 charcoal such as graphene, graphene oxide (GO) and reduced graphene oxide (rGO) have already  
60 provided insight into the eDNA binding at CMs.<sup>22–24</sup> Molecular dynamics simulation suggested that, at  
61 oxygen-lacking CM's such as graphene, dsDNA binds to surface via the terminal base pairs through  $\pi$ –  
62  $\pi$  stacking.<sup>25</sup> dsDNA can bind either using only one termination, with the helix axis perpendicular to  
63 the graphene surface (“standing up”), or with both terminations forming a horseshoe shape, with the  
64 axis mostly parallel to the surface except close to terminations where base pairs are severely  
65 deformed. From studies of oxygen-containing CM's such as GO and rGO, we know that dsDNA can  
66 bind either electrostatically via the negatively phosphate backbone (helix axis parallel to adsorbent  
67 surface - “lying down”) or by  $\pi$ – $\pi$  interaction and hydrogen bonding via the base pairs at the end of  
68 DNA,<sup>26–28</sup> as with graphene. In the absence of electrolytes that reduce electrostatic repulsion between  
69 negatively charged GO or rGO and negatively charged phosphate backbone, bulk adsorption studies  
70 suggest that hydrophobic forces dominate the interaction with DNA.<sup>29</sup> However, in the presence of  
71 electrolytes, electrostatic interaction becomes more important evidenced by increasing DNA  
72 adsorption capacity as the ionic strength increases<sup>29,30</sup> or as pH decreases.<sup>29</sup> The distribution of oxygen  
73 functional groups in GO and rGO is highly heterogeneous,<sup>31,32</sup> *i.e.*, they contain areas that are rich and  
74 areas that are poor in functional groups. The interaction between these surfaces and the phosphate  
75 backbone likely takes place at the areas rich in hydrophilic functional groups. In contrast, the  $\pi$  –  $\pi$   
76 stacking takes place at areas poor in oxygen functional groups (graphene-like). Combined, these  
77 studies suggest that the ratio of hydrophilic and hydrophobic areas in carbonaceous materials  
78 determines their overall interaction with dsDNA, with hydrophobic interactions becoming dominant  
79 in materials rich in graphene-like surfaces. **However, graphene-like materials are rare in the**  
80 **environment and it is unclear to which extent our current understanding of DNA interactions with**  
81 **carbonaceous materials is applicable to environmentally common surfaces such as soot and charcoal.**

82 We determined the composition of soot and charcoal using Scanning Electron Microscopy (SEM), X-  
83 ray Diffraction (XRD) and X-ray Photoelectron Spectroscopy (XPS), the structure using Raman  
84 Spectroscopy, and the surface properties using water vapour adsorption, mass titration and  
85 electrokinetic measurements. To elucidate how structure, composition and surface properties  
86 influence DNA adsorption at soot and charcoal, we measured the adsorption capacity for DNA as a

87 function of pH, ionic strength, solution composition, time and DNA length. We used isotherm  
88 modelling to quantify differences in isotherm shapes. By evaluating how the surface properties of soot  
89 and charcoal influence the adsorption of DNA as a function of solution composition, we infer a likely  
90 adsorption mechanism. We propose that, besides electrostatic forces, hydrophobic interactions play  
91 an important role in adsorption of DNA to soot and charcoal. This information can be used for  
92 improving protocols of eDNA extraction from environmental matrices where soot and charcoal are  
93 abundant such as urban and wildfire aerosol, and topsoil. This is important because DNA adsorbed at  
94 soot and charcoal could hold (paleo)biodiversity information that is not available through routine  
95 eDNA extraction and analysis. Advancing our understanding of interactions between DNA and  
96 environmental surfaces will provide an important contribution to understanding of eDNA reservoirs  
97 in the environment.

## 98 MATERIALS AND METHODS

### 99 Material characterisation

100 We purchased carbon soot nanopowder (NANOSHEL, >98.9%, CAS: 7440-44-0), further called soot,  
101 and activated charcoal (DARCO, Sigma Aldrich), further called charcoal. We used XRD to identify major  
102 and minor contaminants. We collected diffractograms between 5-90 °2 $\theta$  using a Bruker D8  
103 diffractometer equipped with Cu  $K_{\alpha}$  radiation (40 kV, 40 mA;  $\lambda \sim 1.543 \text{ \AA}$ ). We used step size of 0.04  
104 °2 $\theta$ , time per step of 6 s and spun the sample at 20 rpm with 0.3° divergence and antiscatter slit and  
105 2.3° Soller slits on both incident and diffracted beams.

106 We identified trace phases using SEM by fixing powders on a double-sided carbon tape and sputter  
107 coated them with ~1 nm of Au. Images and energy-dispersive spectra were obtained using Vega-3  
108 Tescan microscope. Both images and spectra were collected with a beam operated at 20 kV.

109 The surface elemental composition was determined using XPS. We used double-sided sticky tape to  
110 fix the samples. Wide and high-resolution spectra were collected using PHI X-tool instrument (Physical  
111 Electronics Inc., Chanhassen, MN, USA) (excitation energy  $h\nu = 1486.7 \text{ eV}$ , tension voltage 18 kV,  
112 emission power 52 W) with a spot size of 205  $\mu\text{m}^2$ . The photoelectrons were collected at 45° take-off  
113 angle using a pass energy of 280 eV with a step of 0.25 eV. The spectra calibration was done by  
114 assigning the C1s peak to 284.8 eV.

115 To estimate the structural disorder of soot and charcoal, we used Raman spectroscopy. We spread  
116 the powders on Al-foil and acquired spectra with a 532 nm Ar-laser operated at 100% effect  
117 (approximately 60 mW before the objective) using a WITec alpha 300R confocal Raman microscope  
118 (WITec GmbH). The spectral resolution of the spectrometer (UHTS300 spectrometer VIS) was 3.8  $\text{cm}^{-1}$ .  
119 Each spectrum was obtained as the mean of 100, 0.1 s scans. We removed signal from cosmic rays  
120 by median filtering and corrected the background by an asymmetric least square algorithm. The  
121 spectra were then Savitzky-Golay smoothed to minimise the noise. Each sample was analysed in at  
122 least triplicates. We used a relative intensities of G (~1560  $\text{cm}^{-1}$ ), D1 (~1350  $\text{cm}^{-1}$ ) and D2 (~1600  $\text{cm}^{-1}$ )  
123 bands to estimate the fraction of a ordered graphitic component, *i.e.* the structural order of soot and  
124 charcoal.<sup>33-36</sup> In addition, we calculated R2 parameter to estimate the disorder in soot and charcoal:<sup>37</sup>

$$R2 = \frac{I(D_1)}{I(D_1) + I(G) + I(D_2)}, \quad \text{Eq 1}$$

125 where  $I$  represents an integrated area under the band.

126 To estimate point of zero charge (PZC), we used mass titration.<sup>38,39</sup> We prepared three solutions with  
127 different initial pH ( $pH_0 \sim 11$ ,  $\sim 6$  and  $\sim 3$ ). 15 ml vials contained 5 ml of either 100 mM  $NaNO_3$  (ACS  
128 reagent,  $\geq 99.0\%$ , Fluka) to estimate PZC in an inert background electrolyte, and 5 and 1 mM  $CaCl_2$   
129 (hexahydrate, ACS reagent,  $\geq 99\%$ , Sigma Aldrich) to estimate the effect of divalent cations on PZC. The  
130 pH was adjusted using 0.1 M  $HNO_3$  and 0.1 M  $NaOH$  for  $NaNO_3$  solution, and 0.1 M  $HCl$  (all Fixanal,  
131 Fluka analytical) and 0.1 M  $NaOH$  for  $CaCl_2$  solutions. We then added soot or charcoal powder to reach  
132 a target weight of a solid (wt.%), rotated the vials for  $\sim 2$  h at 30 rpm for suspension to equilibrate and  
133 then measured the suspension pH before adding another batch of powder.

134 For the electrokinetic measurements, we used a suspension of  $1 \text{ mg ml}^{-1}$  of soot and charcoal prepared  
135 with 1 and 5 mM  $CaCl_2$ . We titrated a 10 ml suspension with 0.05 mM  $HCl$  in 0.5  $\mu\text{L}$  steps and  
136 simultaneously recorded pH and  $\zeta$  potential using a Stabino instrument (Colloid Metrics GmbH,  
137 Germany). The instrument contains a PTFE chamber with an oscillating piston that is slightly negatively  
138 charged. A particle solution is added and van der Waal forces cause particle adsorption at the wall,  
139 yet a fraction is immobilized. Due to the movement of the piston a mobile cloud of double layer is  
140 formed and set in motion. Such oscillating ion cloud generates a voltage, which is captured by two  
141 separate electrodes, defining the streaming potential of the solution, which is proportional to the zeta  
142 potential of the particles. The Stabino streaming potential method can measure across a large particle  
143 size range (0.3nm-300 $\mu\text{m}$ ) and particle concentrations up to 40 vol.%. Moreover, optical properties of  
144 the liquid are not relevant for its measurement, unlike electrophoresis method, which may be  
145 challenging when working with soot and charcoal.

146 To estimate a hydrophobic character of soot and charcoal, we volumetrically collected water vapor  
147 isotherms at 25 °C using a BELSORP-MAX instrument from BEL Japan. Prior, powders were outgassed  
148 at 150 °C for 24 h at a residual pressure of  $10^{-5} - 10^{-4}$  Pa.

#### 149 **Batch adsorption experiments**

150 **Materials.** We used low molecular weight salmon sperm double stranded DNA (lyophilised powder,  
151 Sigma Aldrich) with a size of  $\sim 30$  base pairs (bp) because it is easily accessible in large amounts and  
152 concentrations required for obtaining reliable adsorption isotherms. Since 30 bp is on the shorter end  
153 of extracted environmental (ancient) DNA, except for a set of experiments where we looked into the  
154 influence of DNA length on adsorption capacity of soot and charcoal where we used salmon sperm by  
155 comparing it to adsorption of double stranded DNA salmon sperm solution (UltraPure,  $10 \text{ mg ml}^{-1}$ ,  
156 ThermoFischer Scientific) with the size of  $\leq 2000$  bp. We used DNA LoBind tubes (Eppendorf) and  
157 DNase/RNase-free water (molecular biology water, LONZA, AccuGene) for preparation of all solutions  
158 and suspensions. The pH of stocks and suspensions was adjusted with 0.1 M  $HCl$  and 0.1 M  $NaOH$  and  
159 measured with 913 Metrohm metre calibrated on a daily basis (precision  $\pm 0.1$  unit). We did not use  
160 pH buffers as they are known to modify DNA adsorption capacity.<sup>40</sup> We prepared 1 mM and 100 mM  
161 electrolyte stocks of  $NaCl$  (ACS reagent,  $\geq 99\%$ , anhydrous, Sigma Aldrich) and  $CaCl_2$ , and soot and  
162 charcoal stock suspensions at the concentration of  $50 \text{ mg ml}^{-1}$ . Immediately prior to an experiment, we  
163 prepared  $1 \text{ mg ml}^{-1}$  DNA stock (30 bp) by dissolving lyophilised powder in electrolyte suspension,  
164 shaken it for 15 min at 20 °C at 300 rpm on an orbital shaker and adjusted the pH.

165 **Batch equilibrium adsorption.** For adsorption experiments, we mixed 10  $\mu\text{l}$  of a stock suspension (soot  
166 or charcoal) with the predetermined volume of electrolyte solution or pure water in 2 ml tube and  
167 ultrasonicated it for 10 min to break aggregates. We then added DNA stock to a final volume of 1 ml,  
168 vortexed the sample for a couple of seconds and placed it on a revolver rotator (18 rpm). The final  
169 mass concentration of suspensions was 0.5 – 0.6  $\mu\text{g ml}^{-1}$ . To obtain reliable isotherms for adsorption  
170 modelling, we prepared 5-8 different DNA concentrations between 10 – 800  $\mu\text{g ml}^{-1}$ , in triplicates. After

171 6 h of equilibration at room temperature, we centrifuged the tubes for 3 min at 5000 rpm and  
172 separated top 200  $\mu\text{l}$  of the supernatant for UV spectrometry (Biophotometer, Eppendorf) using  
173 microcuvettes (BRAND). To account for turbidity, we determined the DNA concentration by  
174 subtracting the absorbance of the supernatant at 320 nm from the absorbance at 260 nm. To account  
175 for various instrumental uncertainties, the subtracted absorbance was read from a DNA calibration  
176 curve calculated on an everyday basis from freshly prepared DNA standards.

177 When we looked at the influence of pH, solvents (ethanol, BioReagents, absolute, Fisher Scientific;  
178 isopropanol, Bioreagent,  $\geq 99\%$ , Sigma Aldrich), and phosphates (Na-polyphosphate,  $\geq 68\%$   $\text{P}_2\text{O}_5$  basis,  
179 EMPLURA, Supelco; Na-metaphosphate, 96%, Sigma Aldrich) on adsorption, we followed the same  
180 protocol as for isotherms, except that the stock was diluted to only one initial DNA concentration, 50  
181  $\text{mgml}^{-1}$ .

182 **Kinetic experiments.** The kinetic experiments were done using initial DNA concentration of 50  $\text{mgml}^{-1}$   
183  $^1$ , in 100 mM NaCl solution and at three temperatures: 283, 293 and 303 K (Eppendorf ThermoMixer;  
184 precision  $\pm 0.2$  K). To have enough suspension to sample over the course of the experiment, we  
185 upscaled the quantities and used 15 ml instead of 2 ml tubes as was done in adsorption studies. We  
186 equilibrated the suspension and the DNA solution separately for 2 h at desired temperature before  
187 mixing them together to minimise temperature fluctuations over the course of experiment. At various  
188 time intervals (3 min – 29 h), 200  $\mu\text{l}$  of suspension were extracted and centrifuged for 3 min at 5000  
189 rpm and the supernatant was kept for UV measurement. The sampling time reported includes  
190 centrifugation time, i.e. the sampling time of 6 min means that the sample was equilibrated for 3  
191 minutes in thermomixer and then centrifuged for 3 minutes.

192 **Calculation of adsorption capacities.** The equilibrium adsorption capacity of DNA ( $q_{eq}$ ,  $\mu\text{gmg}^{-1}$ ) was  
193 determined as a function of equilibrium DNA concentration in solution ( $c_{eq}$ ,  $\mu\text{gml}^{-1}$ ) by taking:

$$q_{eq} = \frac{c_i - c_{eq}}{\gamma}, \quad \text{Eq 2}$$

194 where  $c_i$  ( $\mu\text{gml}^{-1}$ ) represents the initial concentration of DNA and  $\gamma$  represents the mass concentration  
195 of soot or charcoal ( $\text{mgml}^{-1}$ ). For kinetic experiments, we determined the adsorption capacity  $q_t$  ( $\text{mgml}^{-1}$ )  
196  $^1$  at time  $t$  (min):

$$q_t = c_i - c_t, \quad \text{Eq 3}$$

197 where  $c_t$  ( $\mu\text{gml}^{-1}$ ) represents DNA concentration measured in the supernatant at time  $t$ . Throughout  
198 the paper, we refer to a plot of  $q_{eq}$  vs.  $c_{eq}$  as an adsorption isotherm and to a plot of  $q_t$  vs.  $t$  as kinetic  
199 data.

200 **Modelling of equilibrium adsorption and kinetic data.** We fit the adsorption isotherms using  
201 equations that model monolayer and multilayer adsorption (but acknowledge that such modelling  
202 alone does not reveal how adsorption takes place in reality), and the kinetic data using equations that  
203 model surface and diffusion -controlled processes (Table S1.). We applied nonlinear least squares  
204 regression to fit data to models. We chose the mathematically best fitting most appropriate-model by  
205 comparing their reduced chi-squared parameter of fits,  $\chi^2_v$ , i.e. the  $\chi^2_v$  closest to 1 was considered the  
206 best. If the best fit resulted in standard errors that were larger than the fitting parameters, the fit with  
207  $\chi^2_v$  that was next in line but with standard errors smaller than the fitting parameters was considered  
208 more appropriate, i.e., matching the form of curve better.

## 209 RESULTS AND DISCUSSION

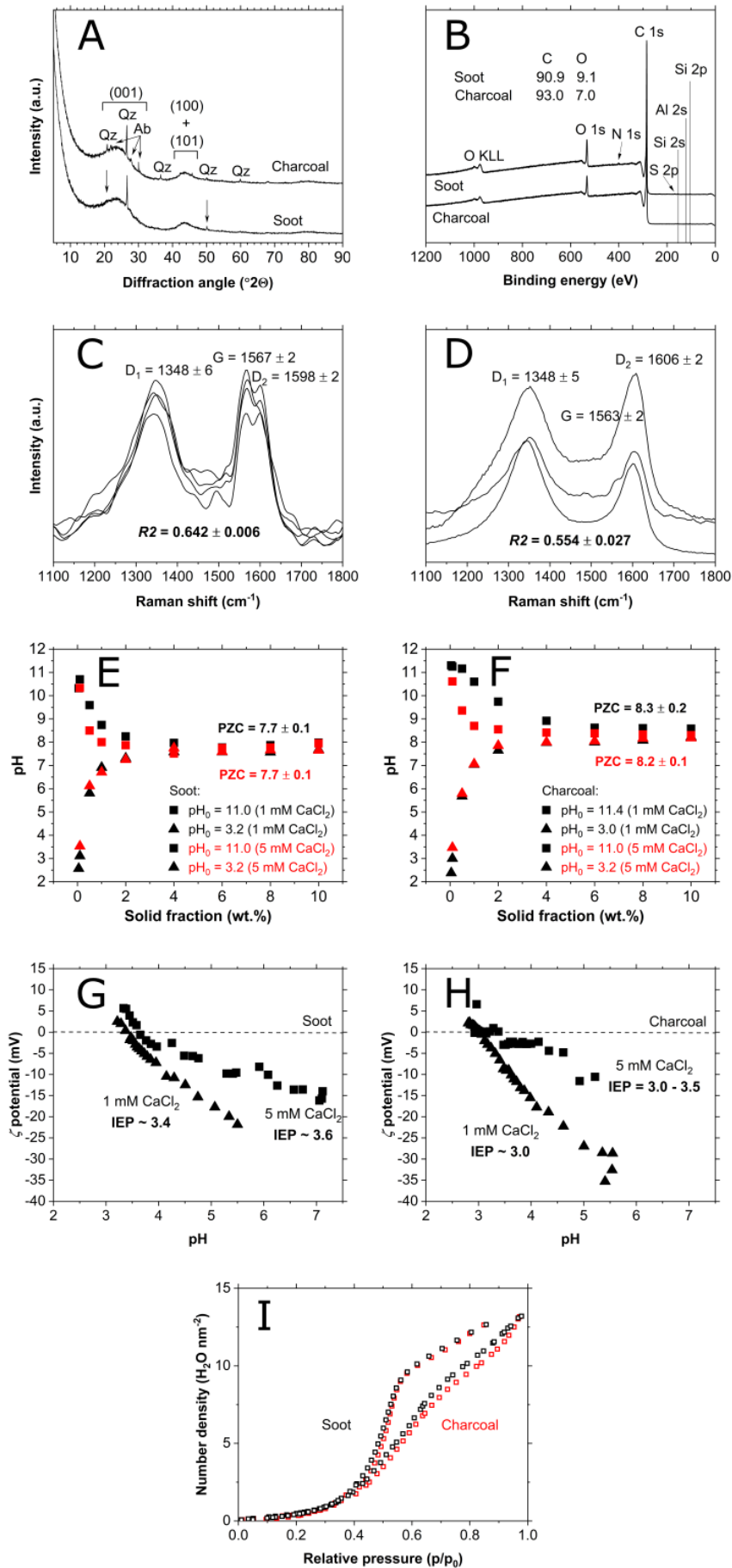
## 210 Composition and properties of soot and charcoal

211 **Phase and elemental composition.** Both soot and charcoal are largely composed of poorly ordered  
212 graphite-like carbon material as evidenced by the presence of broad diffraction peaks between 15 -  
213 30 °2 $\theta$ , corresponding to graphite (001) reflection, and 40 - 50 °2 $\theta$ , corresponding to a combination  
214 of graphite (100) and (101) reflections (Fig. 1A). In addition, soot contains quartz (SiO<sub>2</sub>) as a minor  
215 impurity identified by XRD and trace amounts of titanite (CaTiSiO<sub>5</sub>; Fig. S1a) and chlorapatite  
216 (Ca<sub>5</sub>(PO<sub>4</sub>)<sub>3</sub>Cl; Fig. S1b) identified by EDX spectroscopy. Charcoal contains minor quartz and Na-rich  
217 plagioclase ((Na,Ca)(Al,Si)<sub>4</sub>O<sub>8</sub>) (Fig. 1A), and trace amounts of likely a Ca-Mg carbonate (either Mg-  
218 calcite (CaCO<sub>3</sub>) or dolomite (CaMg(CO<sub>3</sub>)<sub>2</sub>; Fig. S2b), an Fe-O phase (Fig. S2c) and TiO<sub>2</sub> phase (Fig. S2d).  
219 XPS showed that the surface of soot contained 90.9 At.% of C and 9.1 At.% of O with trace amounts of  
220 Si, N and S while charcoal contained 93.0 At.% of C and 7.0 At.% of O with trace amounts of N, Si and  
221 Al (Figure 1B). Since quartz and plagioclase contain Si and Al, the small surface concentration of these  
222 elements confirm that the contribution of mineral impurities to reactions at soot and charcoal surfaces  
223 is likely negligible.

224 **Structural (Raman) properties.** We observed three bands in Raman spectra of soot and charcoal (Fig.  
225 1C-D):  $D_1$  (~1350 cm<sup>-1</sup>),  $G$  (~1560 cm<sup>-1</sup>) and  $D_2$  (~1600 cm<sup>-1</sup>) bands. The band position is comparable  
226 between soot ( $D_1$ = 1348 ± 6 cm<sup>-1</sup>,  $G$ = 1567 ± 2 cm<sup>-1</sup>,  $D_2$ = 1598 ± 2 cm<sup>-1</sup>) (Fig. 1C) and charcoal ( $D_1$ = 1348  
227 ± 5 cm<sup>-1</sup>,  $G$ = 1563 ± 2 cm<sup>-1</sup>,  $D_2$ = 1606 ± 2 cm<sup>-1</sup>) (Fig. 1D). For soot, the  $G$  band is relatively more intense  
228 compared to both  $D_1$  and  $D_2$  than for charcoal suggesting that soot contains larger volume of an  
229 ordered graphitic component.  $R_2$  parameter (Eq. 1) is smaller for soot (0.554 ± 0.027) compared to  
230 charcoal (0.642 ± 0.006) indicating that soot is overall more ordered and more graphite-like than  
231 charcoal.

232 **Surface properties.** In an inert electrolyte (100 mM NaNO<sub>3</sub>), the PZC of soot (8.3 ± 0.1; Fig. S3a) and  
233 charcoal (9.5 ± 0.1; Fig. S3b) was comparable to previous studies on CMs that used mass titration.<sup>41-44</sup>  
234 In CaCl<sub>2</sub> solutions, the PZC was lower than in NaNO<sub>3</sub> for both soot (7.7 ± 0.1; Fig. 1E) and charcoal (8.3  
235 ± 0.2; Fig. 1F) likely reflecting an increase in surface charge density in divalent electrolyte solutions **as**  
236 **a result of cation adsorption**. The IEP for both materials determined by electrokinetic measurements,  
237 however, was significantly lower: for soot, IEP in 1 mM CaCl<sub>2</sub> was ~ 3.4 and in 5 mM CaCl<sub>2</sub> ~ 3.6 (Fig.  
238 1G) while for charcoal it was ~ 3.0 in 1 mM CaCl<sub>2</sub> and 3.0 – 3.5 in 5 mM CaCl<sub>2</sub> (Fig. 1H). The increase of  
239 IEP with an increase in ionic strength reflects a more efficient screening of negatively charged active  
240 sites. **IEP represents a pH value at which the electrokinetic potential equals zero, i.e. particle is not**  
241 **mobile under applied electric field, while PZC represents a pH value at which the net surface potential**  
242 **of all particle surfaces equals zero. Since A higher PZC than IEP is lower than PZC, the surfaces that**  
243 **control the particle mobility (external surfaces) are more negatively charged than particles whose**  
244 **charge has little influence on mobility (internal surfaces) but can still be probed by proton adsorption,**  
245 **i.e. the titration experiment.<sup>43</sup> indicates a**~~The difference between IEP and PZC implies a~~  
246 ~~heterogeneous distribution of surface charges where external particle surfaces are more negatively~~  
247 ~~charged than internal surfaces of both soot and charcoal,<sup>43</sup> and suggesting suggests that both soot~~  
248 ~~and charcoal that both~~ behave as negatively charged surfaces in circumneutral solutions.

249 Both soot and charcoal adsorbed only 2 - 3 molecules of water at low pressures ( $p/p_0 < 0.4$ , Fig. 1I), a  
250 characteristic of hydrophobic surfaces.<sup>45,46</sup> The difference in the adsorbed water between soot and  
251 charcoal is <0.1 molecule/nm, reflecting a similar surface composition determined with XPS (Fig. 1B)  
252 and suggesting no significant difference in bulk hydrophobicity between soot and charcoal.



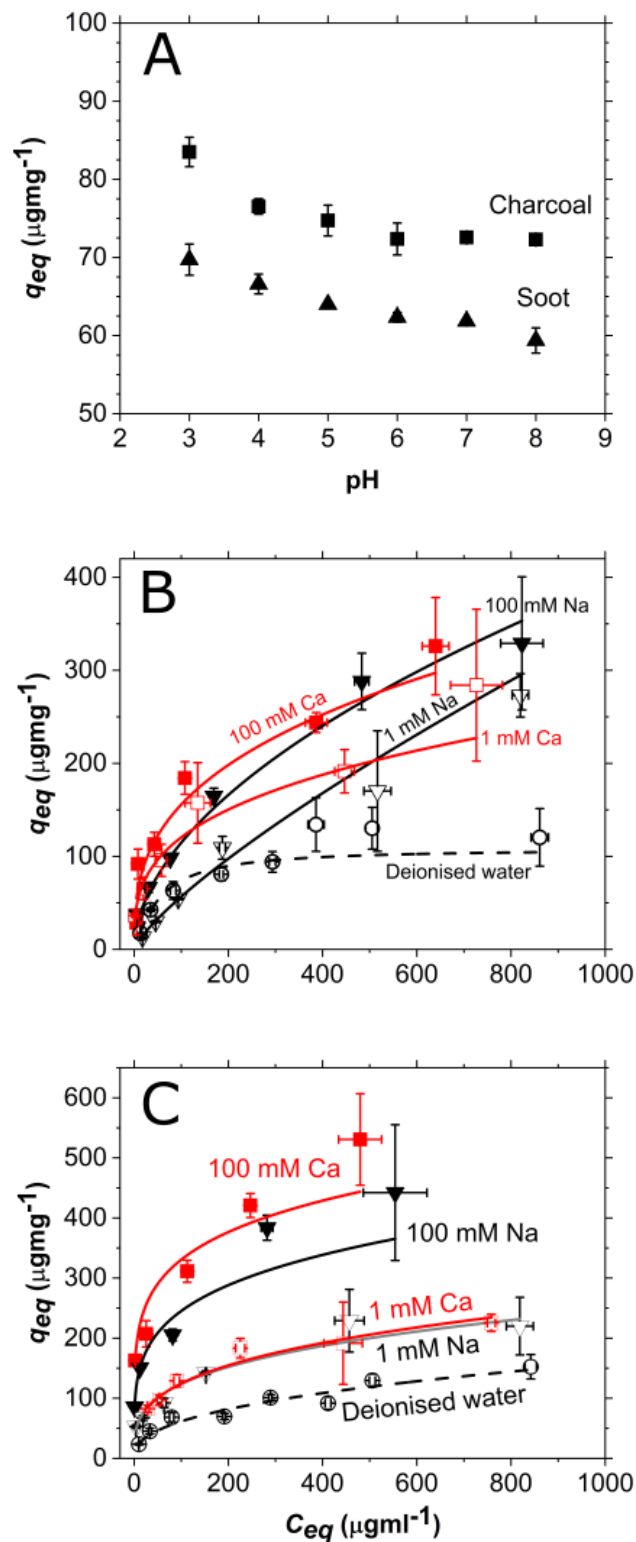
254 Figure 1. a) XRD patterns with assigned diffraction peaks from the graphite structure; Qz – quartz  
255 and Ab- albite occur as minor components. b) XPS results and quantitative analysis with assigned  
256 photoelectron peaks. c) soot and d) charcoal Raman spectra containing peak assignment and their  
257 shift. Uncertainties are reported as a range of detected shifts. Mass titration with e) soot and f)  
258 charcoal started from different initial pH values ( $pH_0$ ). Electrokinetic measurements of g) soot and h)  
259 charcoal with the corresponding isoelectric points (IEP) determined as an average between  
260 neighbouring data points above and below 0 mV. h) Number of H<sub>2</sub>O molecules per surface area is  
261 similar between soot (black) and charcoal (red) as determined from water adsorption  
262 measurements.

## 263 Adsorption

264 **pH dependence.** The equilibrium adsorption capacity ( $q_{eq}$ ) of DNA at soot and charcoal decreases as  
265 pH increases (Figure 2A). The capacity is lowest between  $6 < pH < 8$  (soot= $61 \pm 1 \mu\text{gmg}^{-1}$ , charcoal= $72 \pm 0$   
266  $\mu\text{gmg}^{-1}$ ). At  $pH < 6$ , the capacity increases reaching the maximum at  $pH = 3$  (soot= $70 \pm 2 \mu\text{gmg}^{-1}$ ,  
267 charcoal= $83 \pm 2 \mu\text{gmg}^{-1}$ ). Since the  $pK_a$  of the phosphoester in the backbone of DNA is  $\sim 1$ , and soot and  
268 charcoal behave as negatively charged particles above  $\sim 3$  (Fig. 1G-H), a decrease in adsorption capacity  
269 with an increase in pH suggests that the electrostatic interaction plays a role in the interaction. One  
270 would expect that at circumneutral pH, when both DNA, and soot and charcoal are negatively charged,  
271 the adsorption would be minimal and the capacity would be close to zero. However, a significant  
272 amount of DNA is still adsorbed: at both soot and charcoal there is still  $\sim 86\%$  of DNA of the capacity  
273 at  $pH = 3$ . This cannot be due to adsorption at ~~inner-internal~~ particle surfaces that are more positive  
274 than the ~~outer-external~~ particle surfaces (Figure 1E-F) because the ~~outer-external~~ surfaces are even  
275 more negative at circumneutral pH ( $< -10$  mV, Fig. 1G-H) thus repelling DNA. This suggest that the  
276 electrostatics is not the only interaction governing the adsorption.

277 **Adsorption isotherms.** In all solutions and at all DNA concentrations, the adsorption capacity of  
278 charcoal was higher than that of soot (Figure 2B-C). This is even more pronounced when comparing  
279 the adsorption capacity per surface area since specific surface area of charcoal is smaller ( $923 \text{ m}^2\text{g}^{-1}$ )  
280 than of soot ( $973 \text{ m}^2\text{g}^{-1}$ ) (Table S2). As the equilibrium solution concentration of DNA ( $c_{eq}$ ) increased,  
281  $q_{eq}$  of both soot (Figure 2B) and charcoal (Figure 2C) increased abruptly until  $c_{eq} \sim 100 \mu\text{gmg}^{-1}$  after  
282 which the increase is gradual. Regardless of the cation,  $q_{eq}$  was always higher at high cation  
283 concentration (100 mM—full symbols) than at low (1 mM—empty symbols), likely because of more  
284 efficient screening of electrostatic repulsion between negatively charged DNA, and soot and charcoal  
285 surfaces. The influence of cation valency is not as straightforward. For charcoal, larger  $q_{eq}$  in  $\text{CaCl}_2$  than  
286 in  $\text{NaCl}$  solution was consistently observed in the whole range of  $c_{eq}$ 's. For soot, however, the  $q_{eq}$  was  
287 highest in  $\text{CaCl}_2$  solution below  $c_{eq} \sim 400 \mu\text{gml}^{-1}$  but above  $c_{eq} \sim 450 \mu\text{gml}^{-1}$ ,  $q_{eq}$  was comparable or even  
288 lower in  $\text{CaCl}_2$  than in  $\text{NaCl}$  solution. DNA adsorbed at soot and charcoal even in pure water although  
289 with the lowest  $q_{eq}$  measured. The occurrence of adsorption in pure water, *i.e.* in absence of charge  
290 screening cations again suggest that electrostatic interaction is not the only one governing the  
291 adsorption.





292

293 Figure 2. a) DNA adsorption capacity decreases as pH increases in solution with 100 mM NaCl and  
 294 with initial DNA concentration of  $50 \mu\text{gml}^{-1}$ . Adsorption isotherms for b) soot and c) charcoal.  
 295 Experimental data are represented with symbols and best fits with lines (Freundlich model except  
 296 for soot in 1 mM  $\text{CaCl}_2$  solution and deionised water that was best fit with the Sips model). All  
 297 uncertainties given as standard deviation.

298 To quantitatively describe the measured sorption relationships, we fit a range of models (Table S1) to  
 299 the adsorption isotherms (Figure 2B-C, full lines). Based on  $\chi^2_\nu$  parameter, the best fit was to the  
 300 Freundlich model, except for DNA adsorption at soot in pure water and 1 mM CaCl<sub>2</sub>: in these cases,  
 301 the data was best described with the Sips model (Table S3 and S4). The fit to the Freundlich model  
 302 suggests that the DNA adsorption is a multilayer process<sup>47</sup> and that the surfaces are energetically  
 303 heterogeneous, *i.e.* the surface sites at which the adsorption occurs are not of the same energy and  
 304 abundance. At charcoal, the Freundlich constant,  $K_F$ , and the exponent,  $n$ , are lowest for adsorption  
 305 in pure water (Table S3) suggesting that both the adsorption affinity towards DNA (estimated with  
 306  $K_F$ )<sup>48</sup> and the heterogeneity of the surface (estimated with  $n$ )<sup>48</sup> are lowest when there are no cations  
 307 in solution. The dependence between  $K_F$  and  $n$ , and cation concentration and valency is expected since  
 308 both the surface heterogeneity of a material and the surface charge density vary as a function of ionic  
 309 strength, which influences the surface potential.<sup>49</sup> The surface affinity towards DNA and the charcoal  
 310 surface heterogeneity in the presence of 1 mM is significantly lower than in the presence of 100 mM  
 311 of either Na<sup>+</sup> or Ca<sup>2+</sup>. Thus, the DNA adsorption capacity at charcoal follows the trend (Table S3):

$$q_{eq}(\text{DNA, charcoal}) \rightarrow \text{pure water} < 1 \text{ mM NaCl} \sim 1 \text{ mM CaCl}_2 < 100 \text{ mM NaCl} < 100 \text{ mM CaCl}_2. \quad \text{Eq 4}$$

312 We observed a similar trend for adsorption at soot that was best described with the Freundlich model  
 313 (Table S3):

$$q_{eq}(\text{DNA, soot}) \rightarrow 1 \text{ mM NaCl} < 100 \text{ mM NaCl} < 100 \text{ mM CaCl}_2. \quad \text{Eq 5}$$

314 In contrast, the better fit of isotherms at soot in pure water and 1 mM CaCl<sub>2</sub> to the Sips model suggests  
 315 that the surface is still best described as energetically heterogeneous although DNA adsorption has  
 316 **theoretically happens** as monolayer,<sup>50</sup> *i.e.* there exists a maximum adsorption capacity ( $q_{max}$ ) (Table  
 317 S3).  $q_{max}$ , and in fact  $q_{eq}$  at each  $c_{eq}$ , at soot in 1 mM CaCl<sub>2</sub> solution is ~3.5x higher than in pure water,  
 318 *i.e.*:

$$q_{eq}(\text{DNA, soot}) \rightarrow \text{pure water} < 1 \text{ mM CaCl}_2. \quad \text{Eq 6}$$

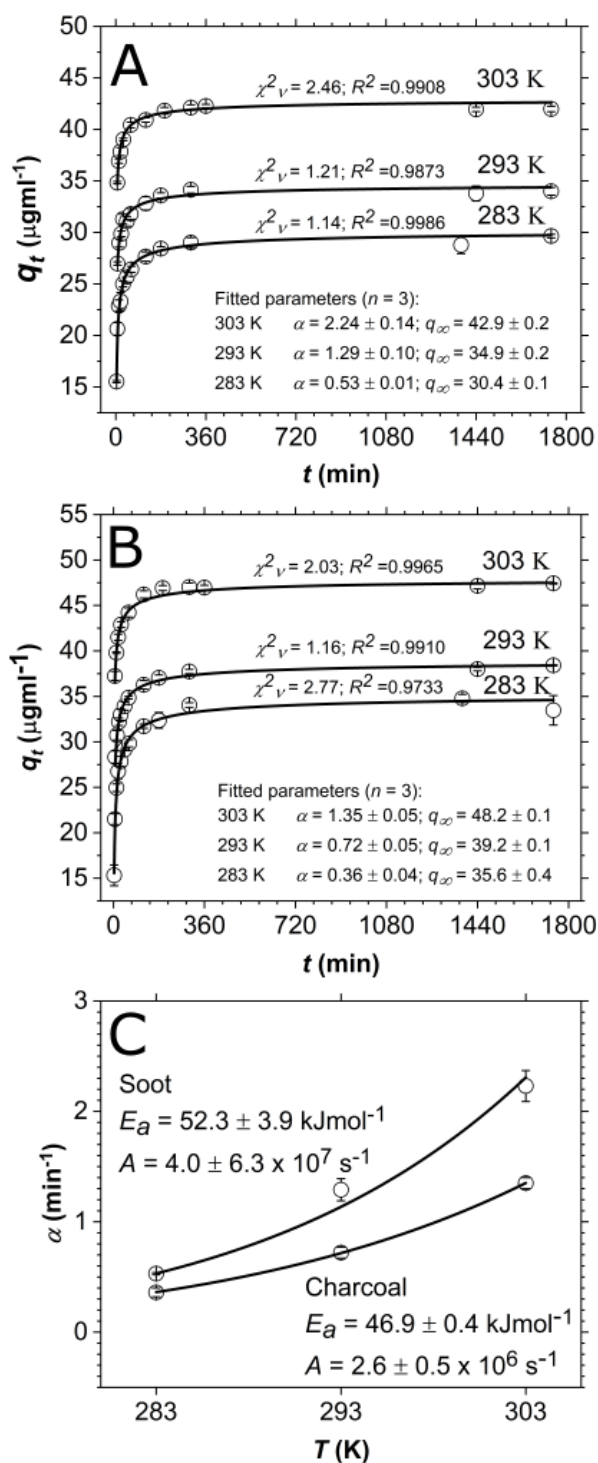
319 A ramification of the Sips equation is that when  $n_s=1$ , the model reduces to the Langmuir equation  
 320 (Table S1) implying that the surface is homogeneous, *i.e.* there is only one type of adsorption site. The  
 321  $n_s=1.16$  for adsorption at soot in pure water suggesting that DNA adsorbs at few adsorption sites. This  
 322 is also corroborated with good fits of the isotherm obtained in pure water to the Langmuir model  
 323 (Table S4). However,  $n_s=0.42$  for adsorption in 1 mM CaCl<sub>2</sub> suggesting that the surface is  
 324 heterogeneous with many adsorption sites. We conclude that, for soot, the surface heterogeneity in  
 325 electrolyte solutions is a consequence of strong ion binding and formation of new sites. In contrast,  
 326 charcoal contains many active sites for DNA adsorption already in pure water and gains more with  
 327 strong ion binding as solution concentration increases.

328 **Adsorption kinetics.** To obtain a more comprehensive insight into the mechanism of DNA adsorption  
 329 at charcoal and soot, we measured the concentration of adsorbed DNA,  $q_t$ , as a function of time,  $t$ , at  
 330 283 K, 293 K and 303 K (Figure 3A-B).  $q_t$  started plateauing at ~300 min suggesting that the equilibrium  
 331 was reached. We continued to monitor the  $q_t$  for another 24 h to obtain a reliable estimates of  $q_t$  at  
 332 infinite time,  $q_\infty$ .

333 Adsorption of DNA at soot and charcoal happens quickly. For soot, half of the DNA adsorbed in <1 min  
 334 at 303 K, ~1 min at 293 K and ~3 min at 283 K (Figure 3A). For charcoal, the adsorption was slower: ~1

335 min at 303 K, ~2 min at 293 K and ~4 min at 283 K (Figure 3B). After 360 min, both soot and charcoal  
336 adsorbed majority of the DNA.

337 To quantitatively assess these observations, we fit the kinetic data to various adsorption kinetic  
338 models (Table S1). The best fit was achieved with the Ritchie 3<sup>rd</sup> order kinetic model (Table S4). This,  
339 however, suggests that the adsorption is not diffusion- but surface-controlled, *i.e.* the mass transfer  
340 depends only on the rate of DNA adsorption on active surface sites and not the rate of its transfer  
341 through the solution to the particle. ~~Based on the assumptions of the Ritchie model,<sup>51</sup> we deduce that  
342 the adsorption is dominated by the interaction with adsorption sites and not by the lateral interactions  
343 between neighbouring molecules and that each DNA molecule occupies three active sites ( $n=3$ ).~~



344

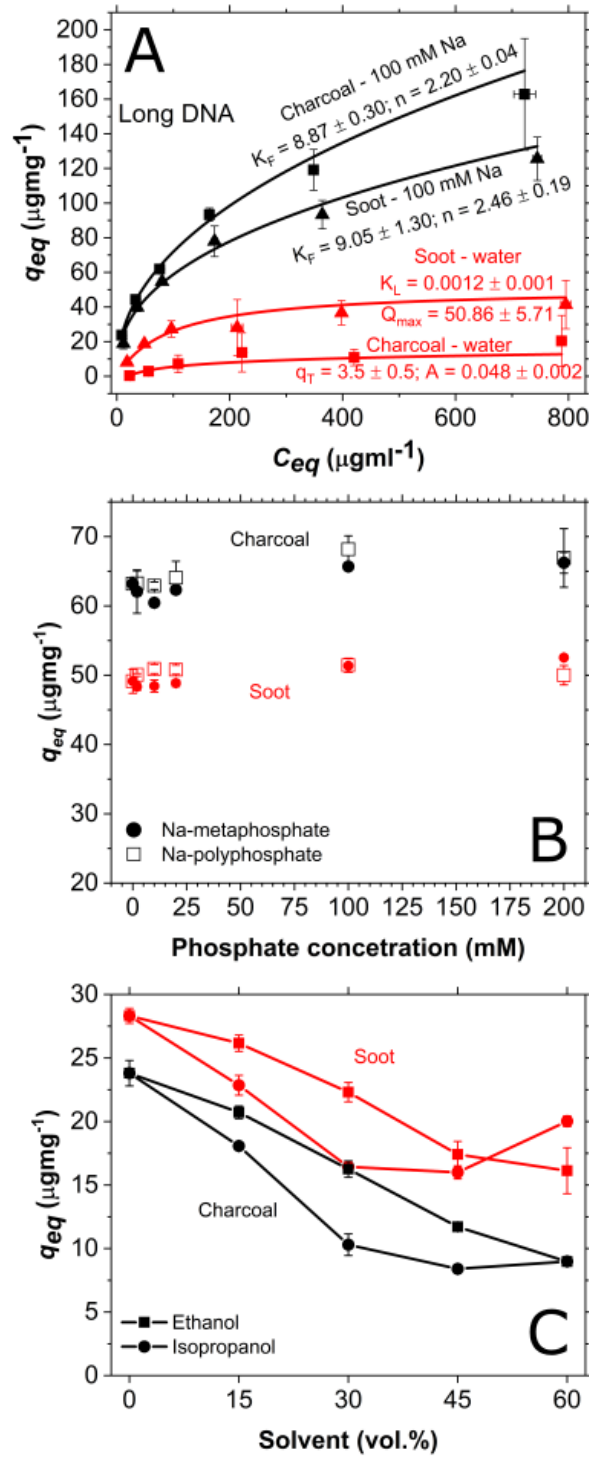
345 Figure 3. Kinetic experimental data (empty circle) with the Ritchie kinetic model (full line),  
 346 corresponding quality of fits ( $\chi^2_{\nu}$ ,  $R^2$ ) and fitted parameters for a) soot and b) charcoal.  $q_{\infty}$  expressed  
 347 in  $\mu\text{gml}^{-1}$  and  $\alpha$  in  $\text{min}^{-1}$ . Adsorption conducted in 100 mM NaCl and pH=7. c) Arrhenius plot derived  
 348 from the kinetic rates (empty circle) showing a logarithmic fit to the data (full line) with the  
 349 calculated adsorption activation energy ( $E_a$ ) and the kinetic pre-factor ( $A$ ). All uncertainties given as  
 350 standard deviation.

351 To estimate the activation energy,  $E_a$ , required for adsorption of DNA at soot and charcoal, we plotted  
352  $\alpha$  as a function of temperature,  $T$  (Figure 3C). We calculated  $E_a$  by fitting the plot to the Arrhenius  
353 equation.<sup>51,52</sup>

$$\alpha = Ae^{\frac{E_a}{RT}}, \quad \text{Eq 7}$$

354 where  $A$  represents kinetic pre-factor ( $\text{min}^{-1}$ ), and  $R$  the gas constant ( $8.3145 \text{ J mol}^{-1}\text{K}^{-1}$ ). We observed  
355 that somewhat higher energy is required to adsorb DNA at soot ( $E_a=52.3 \pm 3.9 \text{ kJmol}^{-1}$ ) than at charcoal  
356 ( $E_a=46.9 \pm 0.4 \text{ kJmol}^{-1}$ ) suggesting that interaction between DNA and soot is stronger than DNA and  
357 charcoal. Given the heterogeneous nature of the active sites at soot and charcoal, the  $E_a$ 's calculated  
358 using the Arrhenius equation are an average of likely many  $E_a$ 's governing DNA adsorption. Regardless,  
359 the  $E_a$ 's are  $>40 \text{ kJmol}^{-1}$ , a rule of thumb value for differentiation between a physisorption and  
360 chemisorption, indicating a strong, perhaps a covalent interaction between DNA, and soot and  
361 charcoal.

362 **Adsorption of long DNA.** In soils, the length of DNA influences the  $q_{eq}$ <sup>52,53,54</sup> and likely the overall  
363 adsorption mechanism. To explore the role of DNA length on adsorption to CMs, we collected  
364 adsorption isotherms using  $<2000 \text{ kb}$  DNA (long DNA) in  $100 \text{ mM NaCl}$  and in pure water (Figure 4A).  
365 Because of charge screening of DNA within the ion atmosphere,<sup>54,55</sup> the DNA in  $100 \text{ mM NaCl}$  is more  
366 coiled compared to DNA in water. Since supercoiled DNA adsorbs less to sand particles compared to  
367 linear or circular DNA,<sup>3</sup> the change in conformation cannot alone explain higher  $q_{eq}$  in  $100 \text{ mM NaCl}$   
368 compared to water. Similarly to  $q_{eq}$  for  $\sim 30 \text{ kb}$  DNA (short DNA) (Figure 2B-C),  $q_{eq}$  for long DNA at  
369 charcoal is larger than at soot in  $100 \text{ mM NaCl}$ . However, this is not the case in pure water where  $q_{eq}$   
370 is higher at soot than at charcoal. This is the only instance where adsorption at soot was higher than  
371 at charcoal (Fig. 2B-C, Table S3). These observations can be explained by enhanced hydrophobic  
372 interactions in pure water compared to electrolytes where charges give rise to electrostatic attractive  
373 interaction.



374

375 Figure 4. A) Adsorption data (symbols) of <2000 bp salmon sperm DNA and the corresponding  
 376 isotherm models (lines). The capacity for long DNA is lower than for short DNA. There is a  
 377 significantly larger difference in the adsorption capacity of DNA in pure water and 100 mM NaCl at  
 378 charcoal than at soot suggesting that different interaction forces control adsorption of DNA at those  
 379 two materials.  $K_F$ =Freundlich constant,  $K_L$ =Langmuir constant,  $Q_{max}$ =maximum adsorption capacity,  
 380  $q_T$ =Temkin capacity,  $A$ =Temkin isotherm constant (units in Table S1). B)  $q_{eq}$  does not significantly vary  
 381 as a function of concentration of Na-polyphosphate and Na-metaphosphate suggesting that  
 382 phosphate backbone of DNA does not play a significant role in adsorption to soot and charcoal.  
 383 Initial DNA concentration  $\sim 50 \mu\text{gml}^{-1}$  (100 mM NaCl). C)  $C_{eq}$  of DNA decreases as the alcohol

384 concentration in the solution increases suggesting hydrophobic interaction plays a role in the DNA  
385 sorption to both materials. Initial DNA concentration was 50  $\mu\text{gml}^{-1}$ . Full lines are not the fit, and  
386 only serve as a guide to the eye. All uncertainties expressed as standard deviation.

387 The fitting to isotherm models revealed very similar behaviour as for the short DNA: The adsorption  
388 of long DNA in electrolytes is best ~~described~~~~explained~~ by a multilayer adsorption ~~model~~~~process~~ for  
389 ~~an~~~~that~~ ~~happens~~ at energetically heterogeneous surface (quality of fit parameters in Table S6, model  
390 fits in Figure 4A). A better fit of the isotherm for charcoal in pure water to Temkin rather than  
391 Freundlich model suggest that there is either a uniform distribution of heterogeneous binding sites or  
392 that there is interaction between neighbouring DNA molecules.<sup>56</sup> Long DNA adsorption at soot in pure  
393 water is still best ~~explained~~~~described~~ by a monolayer adsorption ~~model~~~~but the adsorption sites are~~  
394 ~~energetically similar~~ (Langmuir model). This stands in contrast to ~~adsorption of short DNA that is best~~  
395 ~~described by model for~~ monolayer adsorption ~~of short DNA~~ at heterogeneous surface (Sips model,  
396 Table S3).

397 For long DNA, many of the tested models often fit the data well. Some fits had  $\chi^2_v$  very close to 1 but  
398 the value of standard deviation was larger than the fitted model parameters (red in Table S6). In these  
399 cases, we considered as the best, the fit that had  $\chi^2_v$  next in line but had standard deviation smaller  
400 than the fitted model parameters. The fact that the fitting parameters do not give a conclusive picture  
401 about the adsorption of long DNA suggests that the ~~mechanism~~~~adsorption process~~ is likely more  
402 complicated than in the case of short DNA. However, we did observe that all models that closely fit  
403 experimental data had similar assumptions and implications, *i.e.* adsorption of long DNA at soot in  
404 pure water is similarly well fit with both Langmuir and Toth models (Table S6). Since the z parameter  
405 of Toth model was  $\sim 1$ , this suggests that the adsorption is ~~best described by a model for a~~ monolayer  
406 process but ~~suggesting that the surface is heterogeneous. there might be more than one active site~~  
407 ~~because of the good fit to the Langmuir model.~~

408 Long DNA showed lower  $q_{eq}$  than short DNA both in 100 mM NaCl and pure water. This is a result of  
409 either enhanced steric hindrances as a consequence of size and charge variations of DNA or diffusion  
410 limited mass transfer of long DNA.<sup>52,57</sup> If steric hindrances increase with size, that would suggest that  
411 the phosphate backbone of DNA is responsible for interaction with soot and charcoal surfaces. To test  
412 this, we adsorbed short DNA in presence of polyphosphate and metaphosphate (Figure 4B) that  
413 compete with DNA for adsorption sites at negatively charged surfaces such as clay minerals.<sup>53,58</sup> We  
414 did not observe any changes in  $q_{eq}$  of DNA for a wide range of phosphate concentrations (0-200 mM  
415  $\text{PO}_4^{3-}$  equivalent) suggesting that phosphate backbone is not responsible for DNA interaction with soot  
416 and charcoal, as observed on graphene materials.<sup>29</sup> Since the steric repulsion cannot account for lower  
417  $q_{eq}$  of long compared to short DNA, the alternative explanation by which the adsorption is diffusion  
418 limited implies that a different mechanism controls adsorption of long and short DNA.

419 **Hydrophobic interactions.** To test our hypothesis that the hydrophobic forces play an important role  
420 in DNA adsorption at CM's, we measured the  $q_{eq}$  in mixtures of pure water and ethanol, and pure  
421 water and isopropanol (Figure 4C). These alcohols have lower dielectric constant than water  
422 ( $\epsilon(\text{water})=80$ ,  $\epsilon(\text{ethanol})=25$ ,  $\epsilon(\text{isopropanol})=18$ ) so mixing them decreases the interfacial tension of  
423 water in contact with a hydrophobic surface, decreasing the hydrophobic interactions.<sup>59,60</sup> ~~At ~40%~~  
424 ~~of ethanol, the DNA conformation changes from a B-form predominant in aqueous solution to A-~~  
425 ~~form.<sup>61</sup> The A-form is more compact than B-form and thus likely exhibits a higher charge density. If~~  
426 ~~the electrostatic interaction controls the adsorption of DNA on soot and charcoal, the transition in~~  
427 ~~conformation would suggest an increase in adsorption capacity as the alcohol concentration increases.~~  
428 ~~However, if~~ hydrophobic interactions influence adsorption, water-alcohol mixtures ought to retain  
429 DNA in solution because the entropic drive for partitioning DNA from the solution to the hydrophobic

430 surface is diminished. We observed exactly that, a decrease in DNA adsorption when the volume  
431 fraction of either ethanol or isopropanol in the solution increased (Fig. 4C). In addition, a  $q_{eq}$  in  
432 isopropanol was consistently lower than in ethanol solution, as expected since isopropanol is less polar  
433 than ethanol so there is a lower drive for DNA to escape it. An exception to this is a larger  $q_{eq}$  at 60  
434 vol.% where we likely observed DNA precipitation in isopropanol but not in ethanol since higher ionic  
435 strengths are needed for DNA precipitation in ethanol mixtures.<sup>6264</sup> Such adsorption behaviour was  
436 also observed on graphene oxide,<sup>29</sup> which is significantly more hydrophilic than either soot or charcoal.

437 Since the bulk hydrophobicity of both CM's is similar, the higher  $q_{eq}$  at soot than charcoal in pure water  
438 is perhaps a consequence of a strong heterogeneous distribution of hydrophobic sites at soot. This  
439 heterogeneity at soot is likely reflected in a more complex modeling of DNA adsorption (eqs 5 and 6)  
440 compared to charcoal (eq 4).

## 441 CONCLUSION

442 Elucidating the role of environmentally common CMs such as soot and charcoal in adsorption and  
443 stabilization of eDNA is important for better understanding of its cycling in environment. This study  
444 ~~revealed~~ showed that the adsorption capacity of dsDNA at soot and charcoal in general follows trends  
445 observed at graphene and graphene oxide surfaces. The adsorption capacity of dsDNA increases as pH  
446 decreases and as ionic strength increases, and it is generally higher for solutions containing divalent  
447 compared to monovalent cations. Such behavior reveals that electrostatic interaction contributes to  
448 DNA-CM binding since both soot and charcoal, and DNA are negatively charged at circumneutral pH  
449 but become positive at lower pH. That the adsorption capacity is generally higher for solutions  
450 containing divalent compared to monovalent cations suggests that attraction is, to an extent,  
451 established by charge screening between negatively charged surfaces and DNA. As revealed by  
452 adsorption modeling, the shape of adsorption isotherms in solutions of different pH and composition  
453 was similar but different between short and long DNA suggesting that adsorption mainly depends on  
454 the length of the DNA molecule but less so on the composition of the surface or the solution. However,  
455 the distribution of hydrophobic areas on soot and charcoal surfaces determine the extent to which  
456 the hydrophobic interactions will take place. Both soot and charcoal are similarly hydrophobic as  
457 evidenced by their water adsorption behavior. However, the contribution of hydrophobic interaction  
458 at soot was much stronger suggesting that regions which interact hydrophobically with DNA are more  
459 suitably distributed to allow adsorption compared to the same regions at charcoal. The majority of  
460 dsDNA adsorbs within minutes at both CMs with the activation energy of  $\sim 50 \text{ kJmol}^{-1}$  suggesting a  
461 strong, ~~perhaps covalent~~ binding. DNA that is bound so strongly to a surface likely cannot be desorbed  
462 by common extraction techniques suggesting that a wealth of genomic and ecologic information might  
463 remain hidden in samples after the extraction. Our results imply that dsDNA binds to both CM's by  
464 terminal basepairs and we showed that both electrostatic and hydrophobic interactions are important  
465 contributors to adsorption. The contribution of one or another interaction depends likely on the  
466 relative proportion of graphitic (hydrophobic) surfaces and those populated by oxygen functional  
467 groups. Combined, this study provides a fundamental understanding of dsDNA-CM interactions that  
468 can be used for improving DNA extraction protocols from environmental matrices containing CM. Our  
469 study covers a fraction of complex environmental conditions while future studies can investigate the  
470 interaction between dsDNA and CM in presence of heavy metals or other cellular organic compounds  
471 such as proteins or lipids. Such investigations would contribute to the comprehensive understanding  
472 of cycling of eDNA bound to CM's and its use in biomonitoring.

473 Our results demonstrate that CM's are likely reservoirs of extracellular eDNA in urban aerosol and  
474 topsoil and environments under influence of wildfires. These reservoirs can potentially be used for  
475 monitoring of biodiversity, and invasive and endangered species.

## 476 ACKNOWLEDGMENTS



477 We thank Enrico Cappellini for access to Biophotometer. KKS and SJ are grateful for a research grant  
478 from VILLUM FONDEN (00025352). SJ was partly funded by French Government through MOPGA  
479 Postdoctoral Programme (reference number 3—5402234721). The geochemistry-mineralogy  
480 platform of ISTERre (Grenoble, France) is partially funded by a grant from Labex OSUG@2020  
481 (investissements d’avenir, ANR10-LABX56). SM was funded by the VILLUM FONDEN (Grant numbers  
482 00022942).

#### 483 **CONFLICTS OF INTEREST**

484 Authors declare no conflicts of interest.

#### 485 **REFERENCES:**

- 486 1. Slon, V. *et al.* Neandertal and Denisovan DNA from Pleistocene sediments. *Science* **356**, 605–608  
487 (2017).
- 488 2. Pedersen, M. W. *et al.* Environmental genomics of Late Pleistocene black bears and giant short-  
489 faced bears. *Current Biology* **31**, 2728-2736.e8 (2021).
- 490 3. Romanowski, G., Lorenz, M. G. & Wackernagel, W. Adsorption of plasmid DNA to mineral surfaces  
491 and protection against DNase I. *Appl. Environ. Microbiol.* **57**, 1057–1061 (1991).
- 492 4. Paget, E., Monrozier, L. J. & Simonet, P. Adsorption of DNA on clay minerals: protection against  
493 DNaseI and influence on gene transfer. *FEMS Microbiology Letters* **97**, 31–39 (1992).
- 494 5. Khanna, M. & Stotzky, G. Transformation of *Bacillus subtilis* by DNA bound on montmorillonite  
495 and effect of DNase on the transforming ability of bound DNA. *Appl Environ Microbiol* **58**, 1930–  
496 1939 (1992).
- 497 6. Thomsen, P. F. & Willerslev, E. Environmental DNA – An emerging tool in conservation for  
498 monitoring past and present biodiversity. *Biological Conservation* **183**, 4–18 (2015).
- 499 7. Bohmann, K. *et al.* Environmental DNA for wildlife biology and biodiversity monitoring. *Trends in*  
500 *Ecology & Evolution* **29**, 358–367 (2014).
- 501 8. Pedersen, M. W. *et al.* Ancient and modern environmental DNA. *Philosophical Transactions of the*  
502 *Royal Society B: Biological Sciences* **370**, 20130383 (2015).
- 503 9. Taberlet, P., Bonin, A., Zinger, L. & Coissac, E. *Environmental DNA: For Biodiversity Research and*  
504 *Monitoring.* (Oxford University Press, 2018). doi:10.1093/oso/9780198767220.001.0001.

- 505 10. Clare, E. L. *et al.* Measuring biodiversity from DNA in the air. *Current Biology* **32**, 693-700.e5  
506 (2022).
- 507 11. Lynggaard, C. *et al.* Airborne environmental DNA for terrestrial vertebrate community  
508 monitoring. *Current Biology* **32**, 701-707.e5 (2022).
- 509 12. Schmidt, M. W. I. & Noack, A. G. Black carbon in soils and sediments: Analysis, distribution,  
510 implications, and current challenges. *Global Biogeochemical Cycles* **14**, 777–793 (2000).
- 511 13. Xi, J., Yang, G., Cai, J. & Gu, Z. A Review of Recent Research Results on Soot: The Formation  
512 of a Kind of Carbon-Based Material in Flames. *Frontiers in Materials* **8**, 179 (2021).
- 513 14. Franklin, R. E. & Randall, J. T. Crystallite growth in graphitizing and non-graphitizing carbons.  
514 *Proceedings of the Royal Society of London. Series A. Mathematical and Physical Sciences* **209**,  
515 196–218 (1951).
- 516 15. Sadezky, A., Muckenhuber, H., Grothe, H., Niessner, R. & Pöschl, U. Raman  
517 microspectroscopy of soot and related carbonaceous materials: Spectral analysis and structural  
518 information. *Carbon* **43**, 1731–1742 (2005).
- 519 16. Müller, J.-O., Su, D. S., Wild, U. & Schlögl, R. Bulk and surface structural investigations of  
520 diesel engine soot and carbon black. *Phys. Chem. Chem. Phys.* **9**, 4018–4025 (2007).
- 521 17. Pyle, L. A. *et al.* Chemical and Isotopic Thresholds in Charring: Implications for the  
522 Interpretation of Charcoal Mass and Isotopic Data. *Environ. Sci. Technol.* **49**, 14057–14064 (2015).
- 523 18. Lindahl, T. & Andersson, A. Rate of chain breakage at apurinic sites in double-stranded  
524 deoxyribonucleic acid. *Biochemistry* **11**, 3618–3623 (1972).
- 525 19. Frederico, L. A., Kunkel, T. A. & Shaw, B. R. A sensitive genetic assay for the detection of  
526 cytosine deamination: determination of rate constants and the activation energy. *Biochemistry*  
527 **29**, 2532–2537 (1990).
- 528 20. Impellizzeri, K. J., Anderson, B. & Burgers, P. M. The spectrum of spontaneous mutations in a  
529 *Saccharomyces cerevisiae* uracil-DNA-glycosylase mutant limits the function of this enzyme to  
530 cytosine deamination repair. *J Bacteriol* **173**, 6807–6810 (1991).

- 531 21. Torti, A., Lever, M. A. & Jørgensen, B. B. Origin, dynamics, and implications of extracellular  
532 DNA pools in marine sediments. *Marine Genomics* **24**, 185–196 (2015).
- 533 22. Szabó, T. *et al.* Evolution of Surface Functional Groups in a Series of Progressively Oxidized  
534 Graphite Oxides. *Chem. Mater.* **18**, 2740–2749 (2006).
- 535 23. Knauer, M. *et al.* Soot Structure and Reactivity Analysis by Raman Microspectroscopy,  
536 Temperature-Programmed Oxidation, and High-Resolution Transmission Electron Microscopy. *J.*  
537 *Phys. Chem. A* **113**, 13871–13880 (2009).
- 538 24. Erickson, K. *et al.* Determination of the Local Chemical Structure of Graphene Oxide and  
539 Reduced Graphene Oxide. *Advanced Materials* **22**, 4467–4472 (2010).
- 540 25. Zhao, X. Self-Assembly of DNA Segments on Graphene and Carbon Nanotube Arrays in  
541 Aqueous Solution: A Molecular Simulation Study. *J. Phys. Chem. C* **115**, 6181–6189 (2011).
- 542 26. He, S. *et al.* A Graphene Nanoprobe for Rapid, Sensitive, and Multicolor Fluorescent DNA  
543 Analysis. *Advanced Functional Materials* **20**, 453–459 (2010).
- 544 27. Lei, H. *et al.* Adsorption of double-stranded DNA to graphene oxide preventing enzymatic  
545 digestion. *Nanoscale* **3**, 3888–3892 (2011).
- 546 28. Tang, L., Chang, H., Liu, Y. & Li, J. Duplex DNA/Graphene Oxide Biointerface: From  
547 Fundamental Understanding to Specific Enzymatic Effects. *Advanced Functional Materials* **22**,  
548 3083–3088 (2012).
- 549 29. Wu, M., Kempaiah, R., Huang, P.-J. J., Maheshwari, V. & Liu, J. Adsorption and Desorption of  
550 DNA on Graphene Oxide Studied by Fluorescently Labeled Oligonucleotides. *Langmuir* **27**, 2731–  
551 2738 (2011).
- 552 30. Huang, P.-J. J. & Liu, J. Molecular Beacon Lighting up on Graphene Oxide. *Anal. Chem.* **84**,  
553 4192–4198 (2012).
- 554 31. Liu, Z. *et al.* Direct observation of oxygen configuration on individual graphene oxide sheets.  
555 *Carbon* **127**, 141–148 (2018).

- 556 32. Liu, Z., Rios-Carvajal, T., Ceccato, M. & Hassenkam, T. Nanoscale chemical mapping of  
557 oxygen functional groups on graphene oxide using atomic force microscopy-coupled infrared  
558 spectroscopy. *Journal of Colloid and Interface Science* **556**, 458–465 (2019).
- 559 33. Tuinstra, F. & Koenig, J. L. Raman Spectrum of Graphite. *J. Chem. Phys.* **53**, 1126–1130  
560 (1970).
- 561 34. Beny-Bassez, C. & Rouzaud, J. N. Characterization of Carbonaceous Materials by Correlated  
562 Electron and Optical Microscopy and Raman Microspectroscopy. *Scanning Electron Microscopy*  
563 119–132 (1985).
- 564 35. Wang, Y., Alsmeyer, D. C. & McCreery, R. L. Raman spectroscopy of carbon materials:  
565 structural basis of observed spectra. *Chem. Mater.* **2**, 557–563 (1990).
- 566 36. Sze, S.-K., Siddique, N., Sloan, J. J. & Escibano, R. Raman spectroscopic characterization of  
567 carbonaceous aerosols. *Atmospheric Environment* **35**, 561–568 (2001).
- 568 37. Beyssac, O., Goffé, B., Chopin, C. & Rouzaud, J. N. Raman spectra of carbonaceous material  
569 in metasediments: A new geothermometer. *Journal of Metamorphic Geology* **20**, 859–871 (2002).
- 570 38. Žalac, S. & Kallay, N. Application of mass titration to the point of zero charge determination.  
571 *Journal of Colloid and Interface Science* **149**, 233–240 (1992).
- 572 39. Preočanin, T. & Kallay, N. Application of »Mass Titration« to Determination of Surface  
573 Charge of Metal Oxides. *Croatica Chemica Acta* **71**, 1117–1125 (1998).
- 574 40. Saeki, K., Kunito, T. & Sakai, M. Effect of Tris-HCl Buffer on DNA Adsorption by a Variety of  
575 Soil Constituents. *Microbes and Environments* **26**, 88–91 (2011).
- 576 41. Noh, J. S. & Schwarz, J. A. Estimation of surface ionization constants for amphoteric solids.  
577 *Journal of Colloid and Interface Science* **139**, 139–148 (1990).
- 578 42. Bandosz, T. J., Jagiello, Jacek. & Schwarz, J. A. Comparison of methods to assess surface  
579 acidic groups on activated carbons. *Anal. Chem.* **64**, 891–895 (1992).

- 580 43. Menéndez, J. A., Illán-Gómez, M. J., y León, C. A. L. & Radovic, L. R. On the difference  
581 between the isoelectric point and the point of zero charge of carbons. *Carbon* **33**, 1655–1657  
582 (1995).
- 583 44. Karanfil, T. & Kilduff, J. E. Role of Granular Activated Carbon Surface Chemistry on the  
584 Adsorption of Organic Compounds. 1. Priority Pollutants. *Environ. Sci. Technol.* **33**, 3217–3224  
585 (1999).
- 586 45. Popovicheva, O. *et al.* Water interaction with hydrophobic and hydrophilic soot particles.  
587 *Phys. Chem. Chem. Phys.* **10**, 2332–2344 (2008).
- 588 46. Liu, L. *et al.* Water adsorption on carbon - A review. *Advances in Colloid and Interface Science*  
589 **250**, 64–78 (2017).
- 590 47. Freundlich, H. Über die Adsorption in Lösungen. *Zeitschrift für Physikalische Chemie* **57U**,  
591 385–470 (1907).
- 592 48. Schwarzenbach, R. P., Gschwend, P. M. & Imboden, D. M. *Environmental Organic Chemistry*.  
593 (John Wiley & Sons, 2016).
- 594 49. Grahame, D. C. Diffuse Double Layer Theory for Electrolytes of Unsymmetrical Valence  
595 Types. *J. Chem. Phys.* **21**, 1054–1060 (1953).
- 596 50. Sips, R. On the Structure of a Catalyst Surface. *J. Chem. Phys.* **16**, 490–495 (1948).
- 597 51. Arrhenius, S. Über die Reaktionsgeschwindigkeit bei der Inversion von Rohrzucker durch  
598 Säuren. *Zeitschrift für Physikalische Chemie* **4U**, 226–248 (1889).
- 599 52. Ogram, A. V., Mathot, M. L., Harsh, J. B., Boyle, J. & Pettigrew, C. A. Effects of DNA Polymer  
600 Length on Its Adsorption to Soils. *Appl Environ Microbiol* **60**, 393–396 (1994).
- 601 53. Pietramellara, G., Franchi, M., Gallori, E. & Nannipieri, P. Effect of molecular characteristics  
602 of DNA on its adsorption and binding on homoionic montmorillonite and kaolinite. *Biol Fertil Soils*  
603 **33**, 402–409 (2001).
- 604 54. Jacobson, D. R. & Saleh, O. A. Counting the ions surrounding nucleic acids. *Nucleic Acids*  
605 *Research* **45**, 1596–1605 (2017).

- 606 55. Lipfert, J., Doniach, S., Das, R. & Herschlag, D. Understanding Nucleic Acid–Ion Interactions.  
607 *Annual Review of Biochemistry* **83**, 813–841 (2014).
- 608 56. Pursell, C. J., Hartshorn, H., Ward, T., Chandler, B. D. & Boccuzzi, F. Application of the Temkin  
609 Model to the Adsorption of CO on Gold. *J. Phys. Chem. C* **115**, 23880–23892 (2011).
- 610 57. Franchi, M. *et al.* Clay-Nucleic Acid Complexes: Characteristics and Implications for the  
611 Preservation of Genetic Material in Primeval Habitats. *Orig Life Evol Biosph* **29**, 297–315 (1999).
- 612 58. Saeki, K., Kunito, T. & Sakai, M. Effects of pH, ionic strength, and solutes on DNA adsorption  
613 by andosols. *Biol Fertil Soils* **46**, 531–535 (2010).
- 614 59. Yaacobi, M. & Ben-Naim, A. Hydrophobic interaction in water-ethanol mixtures. *J Solution*  
615 *Chem* **2**, 425–443 (1973).
- 616 60. Ballal, D. & Chapman, W. G. Hydrophobic and hydrophilic interactions in aqueous mixtures  
617 of alcohols at a hydrophobic surface. *J. Chem. Phys.* **139**, 114706 (2013).
- 618 61. Marchetti, S., Onori, G. & Cametti, C. Ethanol-induced compaction of DNA: a viscosimetry  
619 and dynamic light scattering study. *Philosophical Magazine* **87**, 525–534 (2007).
- 620 62. Herskovits, T. T. Nonaqueous solutions of DNA: Factors determining the stability of the  
621 helical configuration in solution. *Archives of Biochemistry and Biophysics* **97**, 474–484 (1962).
- 622 ~~1. Slon, V. *et al.* Neandertal and Denisovan DNA from Pleistocene sediments. *Science* **356**, 605–608~~  
623 ~~(2017).~~
- 624 ~~2. Pedersen, M. W. *et al.* Environmental genomics of Late Pleistocene black bears and giant short-~~  
625 ~~faced bears. *Current Biology* **31**, 2728–2736.e8 (2021).~~
- 626 ~~3. Romanowski, G., Lorenz, M. G. & Wackernagel, W. Adsorption of plasmid DNA to mineral surfaces~~  
627 ~~and protection against DNase I. *Appl. Environ. Microbiol.* **57**, 1057–1061 (1991).~~
- 628 ~~4. Paget, E., Monrozier, L. J. & Simonet, P. Adsorption of DNA on clay minerals: protection against~~  
629 ~~DNaseI and influence on gene transfer. *FEMS Microbiology Letters* **97**, 31–39 (1992).~~

- 630 5. Khanna, M. & Stotzky, G. Transformation of *Bacillus subtilis* by DNA bound on montmorillonite  
631 and effect of DNase on the transforming ability of bound DNA. *Appl Environ Microbiol* **58**, 1930–  
632 1939 (1992).
- 633 6. Thomsen, P. F. & Willerslev, E. Environmental DNA—An emerging tool in conservation for  
634 monitoring past and present biodiversity. *Biological Conservation* **183**, 4–18 (2015).
- 635 7. Bohmann, K. *et al.* Environmental DNA for wildlife biology and biodiversity monitoring. *Trends in*  
636 *Ecology & Evolution* **29**, 358–367 (2014).
- 637 8. Pedersen, M. W. *et al.* Ancient and modern environmental DNA. *Philosophical Transactions of the*  
638 *Royal Society B: Biological Sciences* **370**, 20130383 (2015).
- 639 9. Taberlet, P., Bonin, A., Zinger, L. & Coissac, E. *Environmental DNA: For Biodiversity Research and*  
640 *Monitoring*. (Oxford University Press, 2018). doi:10.1093/oso/9780198767220.001.0001.
- 641 10. ——— Clare, E. L. *et al.* Measuring biodiversity from DNA in the air. *Current Biology* **32**, 693–700.e5  
642 (2022).
- 643 11. ——— Lynggaard, C. *et al.* Airborne environmental DNA for terrestrial vertebrate community  
644 monitoring. *Current Biology* **32**, 701–707.e5 (2022).
- 645 12. ——— Schmidt, M. W. I. & Noack, A. G. Black carbon in soils and sediments: Analysis, distribution,  
646 implications, and current challenges. *Global Biogeochemical Cycles* **14**, 777–793 (2000).
- 647 13. ——— Xi, J., Yang, G., Cai, J. & Gu, Z. A Review of Recent Research Results on Soot: The Formation  
648 of a Kind of Carbon-Based Material in Flames. *Frontiers in Materials* **8**, 179 (2021).
- 649 14. ——— Franklin, R. E. & Randall, J. T. Crystallite growth in graphitizing and non-graphitizing carbons.  
650 *Proceedings of the Royal Society of London. Series A. Mathematical and Physical Sciences* **209**,  
651 196–218 (1951).
- 652 15. ——— Sadezky, A., Muckenhuber, H., Grothe, H., Niessner, R. & Pöschl, U. Raman  
653 microspectroscopy of soot and related carbonaceous materials: Spectral analysis and structural  
654 information. *Carbon* **43**, 1731–1742 (2005).

- 655 16. — Müller, J. O., Su, D. S., Wild, U. & Schlögl, R. Bulk and surface structural investigations of  
656 diesel-engine soot and carbon black. *Phys. Chem. Chem. Phys.* **9**, 4018–4025 (2007).
- 657 17. — Pyle, L. A. *et al.* Chemical and Isotopic Thresholds in Charring: Implications for the  
658 Interpretation of Charcoal Mass and Isotopic Data. *Environ. Sci. Technol.* **49**, 14057–14064 (2015).
- 659 18. — Lindahl, T. & Andersson, A. Rate of chain breakage at apurinic sites in double-stranded  
660 deoxyribonucleic acid. *Biochemistry* **11**, 3618–3623 (1972).
- 661 19. — Frederico, L. A., Kunkel, T. A. & Shaw, B. R. A sensitive genetic assay for the detection of  
662 cytosine deamination: determination of rate constants and the activation energy. *Biochemistry*  
663 **29**, 2532–2537 (1990).
- 664 20. — Impellizzeri, K. J., Anderson, B. & Burgers, P. M. The spectrum of spontaneous mutations in a  
665 *Saccharomyces cerevisiae* uracil-DNA-glycosylase mutant limits the function of this enzyme to  
666 cytosine deamination repair. *J. Bacteriol.* **173**, 6807–6810 (1991).
- 667 21. — Torti, A., Lever, M. A. & Jørgensen, B. B. Origin, dynamics, and implications of extracellular  
668 DNA pools in marine sediments. *Marine Genomics* **24**, 185–196 (2015).
- 669 22. — Szabó, T. *et al.* Evolution of Surface Functional Groups in a Series of Progressively Oxidized  
670 Graphite Oxides. *Chem. Mater.* **18**, 2740–2749 (2006).
- 671 23. — Knauer, M. *et al.* Soot Structure and Reactivity Analysis by Raman Microspectroscopy,  
672 Temperature-Programmed Oxidation, and High-Resolution Transmission Electron Microscopy. *J.*  
673 *Phys. Chem. A* **113**, 13871–13880 (2009).
- 674 24. — Erickson, K. *et al.* Determination of the Local Chemical Structure of Graphene Oxide and  
675 Reduced Graphene Oxide. *Advanced Materials* **22**, 4467–4472 (2010).
- 676 25. — Zhao, X. Self-Assembly of DNA Segments on Graphene and Carbon-Nanotube Arrays in  
677 Aqueous Solution: A Molecular Simulation Study. *J. Phys. Chem. C* **115**, 6181–6189 (2011).
- 678 26. — He, S. *et al.* A Graphene Nanoprobe for Rapid, Sensitive, and Multicolor Fluorescent DNA  
679 Analysis. *Advanced Functional Materials* **20**, 453–459 (2010).



- 680 27. — Lei, H. *et al.* Adsorption of double-stranded DNA to graphene oxide preventing enzymatic  
681 digestion. *Nanoscale* **3**, 3888–3892 (2011).
- 682 28. — Tang, L., Chang, H., Liu, Y. & Li, J. Duplex DNA/Graphene Oxide Biointerface: From  
683 Fundamental Understanding to Specific Enzymatic Effects. *Advanced Functional Materials* **22**,  
684 3083–3088 (2012).
- 685 29. — Wu, M., Kempaiah, R., Huang, P.-J. J., Maheshwari, V. & Liu, J. Adsorption and Desorption of  
686 DNA on Graphene Oxide Studied by Fluorescently Labeled Oligonucleotides. *Langmuir* **27**, 2731–  
687 2738 (2011).
- 688 30. — Huang, P.-J. J. & Liu, J. Molecular Beacon Lighting up on Graphene Oxide. *Anal. Chem.* **84**,  
689 4192–4198 (2012).
- 690 31. — Liu, Z. *et al.* Direct observation of oxygen configuration on individual graphene oxide sheets.  
691 *Carbon* **127**, 141–148 (2018).
- 692 32. — Liu, Z., Rios-Carvajal, T., Ceccato, M. & Hassenkam, T. Nanoscale chemical mapping of  
693 oxygen functional groups on graphene oxide using atomic force microscopy-coupled infrared  
694 spectroscopy. *Journal of Colloid and Interface Science* **556**, 458–465 (2019).
- 695 33. — Tuinstra, F. & Koenig, J. L. Raman Spectrum of Graphite. *J. Chem. Phys.* **53**, 1126–1130  
696 (1970).
- 697 34. — Beny-Bassez, C. & Rouzaud, J. N. Characterization of Carbonaceous Materials by Correlated  
698 Electron and Optical Microscopy and Raman Microspectroscopy. *Scanning Electron Microscopy*  
699 119–132 (1985).
- 700 35. — Wang, Y., Alsmeyer, D. C. & McCreery, R. L. Raman spectroscopy of carbon materials:  
701 structural basis of observed spectra. *Chem. Mater.* **2**, 557–563 (1990).
- 702 36. — Sze, S.-K., Siddique, N., Sloan, J. J. & Escribano, R. Raman spectroscopic characterization of  
703 carbonaceous aerosols. *Atmospheric Environment* **35**, 561–568 (2001).
- 704 37. — Beyssac, O., Goffé, B., Chopin, C. & Rouzaud, J. N. Raman spectra of carbonaceous material  
705 in metasediments: A new geothermometer. *Journal of Metamorphic Geology* **20**, 859–871 (2002).

- 706 38. — Žalac, S. & Kallay, N. Application of mass titration to the point of zero charge determination.  
707 *Journal of Colloid and Interface Science* **149**, 233–240 (1992).
- 708 39. — Preočanin, T. & Kallay, N. Application of »Mass Titration« to Determination of Surface  
709 Charge of Metal Oxides. *Croatica Chemica Acta* **71**, 1117–1125 (1998).
- 710 40. — Saeki, K., Kunito, T. & Sakai, M. Effect of Tris-HCl Buffer on DNA Adsorption by a Variety of  
711 Soil Constituents. *Microbes and Environments* **26**, 88–91 (2011).
- 712 41. — Noh, J. S. & Schwarz, J. A. Estimation of surface ionization constants for amphoteric solids.  
713 *Journal of Colloid and Interface Science* **139**, 139–148 (1990).
- 714 42. — Bandoz, T. J., Jagiello, Jacek. & Schwarz, J. A. Comparison of methods to assess surface  
715 acidic groups on activated carbons. *Anal. Chem.* **64**, 891–895 (1992).
- 716 43. — Menéndez, J. A., Illán-Gómez, M. J., y León, C. A. L. & Radovic, L. R. On the difference  
717 between the isoelectric point and the point of zero charge of carbons. *Carbon* **33**, 1655–1657  
718 (1995).
- 719 44. — Karanfil, T. & Kilduff, J. E. Role of Granular Activated Carbon Surface Chemistry on the  
720 Adsorption of Organic Compounds. 1. Priority Pollutants. *Environ. Sci. Technol.* **33**, 3217–3224  
721 (1999).
- 722 45. — Popovicheva, O. *et al.* Water interaction with hydrophobic and hydrophilic soot particles.  
723 *Phys. Chem. Chem. Phys.* **10**, 2332–2344 (2008).
- 724 46. — Liu, L. *et al.* Water adsorption on carbon—A review. *Advances in Colloid and Interface Science*  
725 **250**, 64–78 (2017).
- 726 47. — Freundlich, H. Über die Adsorption in Lösungen. *Zeitschrift für Physikalische Chemie* **57U**,  
727 385–470 (1907).
- 728 48. — Schwarzenbach, R. P., Gschwend, P. M. & Imboden, D. M. *Environmental Organic Chemistry*.  
729 (John Wiley & Sons, 2016).
- 730 49. — Grahame, D. C. Diffuse Double Layer Theory for Electrolytes of Unsymmetrical Valence  
731 Types. *J. Chem. Phys.* **21**, 1054–1060 (1953).

- 732 50. — Sips, R. On the Structure of a Catalyst Surface. *J. Chem. Phys.* **16**, 490–495 (1948).
- 733 51. — Arrhenius, S. Über die Reaktionsgeschwindigkeit bei der Inversion von Rohrzucker durch  
734 Säuren. *Zeitschrift für Physikalische Chemie* **4U**, 226–248 (1889).
- 735 52. — Ogram, A. V., Mathot, M. L., Harsh, J. B., Boyle, J. & Pettigrew, C. A. Effects of DNA Polymer  
736 Length on Its Adsorption to Soils. *Appl Environ Microbiol* **60**, 393–396 (1994).
- 737 53. — Pietramellara, G., Franchi, M., Gallori, E. & Nannipieri, P. Effect of molecular characteristics  
738 of DNA on its adsorption and binding on homoionic montmorillonite and kaolinite. *Biol Fertil Soils*  
739 **33**, 402–409 (2001).
- 740 54. — Jacobson, D. R. & Saleh, O. A. Counting the ions surrounding nucleic acids. *Nucleic Acids*  
741 *Research* **45**, 1596–1605 (2017).
- 742 55. — Lipfert, J., Doniach, S., Das, R. & Herschlag, D. Understanding Nucleic Acid–Ion Interactions.  
743 *Annual Review of Biochemistry* **83**, 813–841 (2014).
- 744 56. — Pursell, C. J., Hartshorn, H., Ward, T., Chandler, B. D. & Boccuzzi, F. Application of the Temkin  
745 Model to the Adsorption of CO on Gold. *J. Phys. Chem. C* **115**, 23880–23892 (2011).
- 746 57. — Franchi, M. *et al.* Clay–Nucleic Acid Complexes: Characteristics and Implications for the  
747 Preservation of Genetic Material in Primeval Habitats. *Orig Life Evol Biosph* **29**, 297–315 (1999).
- 748 58. — Saeki, K., Kunito, T. & Sakai, M. Effects of pH, ionic strength, and solutes on DNA adsorption  
749 by andosols. *Biol Fertil Soils* **46**, 531–535 (2010).
- 750 59. — Yaacobi, M. & Ben-Naim, A. Hydrophobic interaction in water–ethanol mixtures. *J Solution*  
751 *Chem* **2**, 425–443 (1973).
- 752 60. — Ballal, D. & Chapman, W. G. Hydrophobic and hydrophilic interactions in aqueous mixtures  
753 of alcohols at a hydrophobic surface. *J. Chem. Phys.* **139**, 114706 (2013).
- 754 61. — Herskovits, T. T. Nonaqueous solutions of DNA: Factors determining the stability of the  
755 helical configuration in solution. *Archives of Biochemistry and Biophysics* **97**, 474–484 (1962).
- 756